Applied Catalysis B: Environmental 95 (2010) 160–168

Contents lists available at ScienceDirect

Applied Catalysis B: Environmental

journal homepage: www.elsevier.com/locate/apcatb

Sulfur poisoning resistant mesoporous Mn-base catalyst for low-temperature SCR of NO with NH_3

Jian Yu [a], Feng Guo [b], Yingli Wang [a], Jianhong Zhu [c], Yunyi Liu [b], Fabing Su [a], Shiqiu Gao [a,*], Guangwen Xu [a,*]

[a] State Key Laboratory of Multi-phase Complex System, Institute of Process Engineering, Chinese Academy of Sciences, Beijing 100190, China
[b] School of Chemical Engineering, Shenyang Institute of Chemical Technology, Shenyang, Liaoning 110142, China
[c] Chemical Engineering Institute of Xiangtan University in Hunan Province, Xiangtan 411105, China

ARTICLE INFO

Article history:
Received 8 September 2009
Received in revised form 10 December 2009
Accepted 18 December 2009
Available online 28 December 2009

Keywords:
Mesoporous catalyst
Manganese
Low-temperature SCR
SO_2 poisoning
Mechanism

ABSTRACT

Mesoporous MnO_2-Fe_2O_3-CeO_2-TiO_2 was prepared with sol–gel method and demonstrated to have good low-temperature activity and sulfur-poisoning resistance for selective catalytic reduction (SCR) of NO with NH_3 in SO_2-containing gases. In comparison with this, the catalyst with the same composition but made according to the conventional impregnation method exhibited obviously lower SO_2-poisoning resistance and selectivity to the formation of N_2 in the SCR reactions. FTIR analysis of the spent catalysts after SCR reactions for 16 h and 60 h in a SO_2-contaning gas demonstrated that there was little difference in the amount of deposited ammonium sulfate over the mesoporous catalyst between the two cases. The mesopore channels existing in the mesoporous catalyst enabled probably a dynamic balance between the formation and decomposition of ammonium sulfate in SCR reactions. This concern was justified through comparing the N_2 adsorptions and XPS spectra for the catalysts made with the impregnation and sol–gel methods. The article clarified as well the facilitation effects of introducing Ce and Fe into the mesoporous catalyst on activity, selectivity and SO_2-poisoning resistance.

1. Introduction

Selective catalytic reduction (SCR) of NO with NH_3 in the presence of residual oxygen (about 2–6 vol.%) is the dominant technology for control of NO from stationary sources such as power boilers and combustion furnaces. The involved major reaction is

$$4NH_3 + 4NO + O_2 \rightarrow 4N_2 + 6H_2O,$$

and V_2O_5-MoO_3/TiO_2 and V_2O_5-WO_3/TiO_2 are the catalysts commonly adopted. These catalysts have high activity for NO reduction and low sensitivity towards SO_2 poisoning [1–5]. However, their working temperatures have to be in 350–400 °C in order to avoid plugging of pores by the deposited ammonium sulfate on the catalyst. This makes the denitration SCR unit have to be installed between the economizer and air preheater in a power boiler system and causes the technology hardly applicable to many industrial furnaces that have flue gas exhaust temperatures varying in 200–300 °C. Meanwhile, at high working temperatures the flue gas has large volume to lead the SCR unit to have large reactor and high capital cost. The development of low-temperature SCR catalysts working at 200–300 °C has received great attention worldwide in past decades. Low-temperature SCR catalyst allows also the easy retrofit of an existing boiler, which is particularly important to China because most of the existing boilers in the country do not have enough space reserved for the installation of a denitration SCR unit working at 350–400 °C. Furthermore, in China the NO_x released from various industrial combustion utilities other than power boilers takes about 30% of the nation's total NO_x emission, having thus large demand for the low-temperature denitration SCR technology working at about 250 °C. This kind of low-temperature SCR technology is necessarily demanded also by the low-load operation situations of a power boiler which may lower the flue gas temperature before the economizer to about 300 °C.

Manganese has been demonstrated to have good low-temperature activity for SCR of NO with NH_3 [6], and various Mn-base catalysts have been prepared and tested in the literature [7–9]. However, these Mn-base catalysts were prepared usually with the impregnation approach and were prone to be easily deactivated by SO_2 present in the treated flue gas. Thus, except of V_2O_5/AC catalyst [10–11], there is still no low-temperature SCR Mn-based catalyst available for practical application to SO_2-containing flue gases. The key issues proved for the SO_2 poisoning in the low-temperature

* Corresponding authors. Tel.: +86 10 62550075; fax: +86 10 62550075.
E-mail addresses: yujian@home.ipe.ac.cn (J. Yu), sqgao@home.ipe.ac.cn (S. Gao), gwxu@home.ipe.ac.cn (s.$. Xu).

0926-3373/$ – see front matter.
doi:10.1016/j.apcatb.2009.12.023

SCR of NO with NH_3 were the formation of ammonium or metal sulfate at the temperatures lower than 350 °C [12]. Tong and co-workers [13] had reported that manganese impregnated on mesoporous silica possessed good SO_2 resistance during a short-time test of the SCR reactions. Nonetheless, no work has been carried out on Mn-base SCR catalyst supported on in situ synthesized mesoporous titanium oxide.

This study suggested that the pore structure and oxidative property of the SCR catalyst would be closely related to the catalyst's capability to resist SO_2 poisoning in SCR. The sol–gel method using amphoteric surfactant as the structure directing agent (SDA) in one-pot reaction was thus devised to prepare a novel Mn-base catalyst. The catalyst exhibited greatly improved resistance to SO_2 poisoning in SCR of NO at about 240 °C. Characterization with N_2 adsorption, XRD, SEM, TEM, FTIR and XPS for the catalysts prepared with the sol–gel and impregnation methods resulted in a deep understanding of the mechanisms for SO_2 poisoning and SCR activity stability at low temperatures.

2. Experimental

2.1. Catalyst preparation

Manganese-base catalysts were prepared with both a newly devised one-pot sol–gel method involving the use of surfactants and the conventional one-pot impregnation method. The catalysts made with the new sol–gel method included MnO_2-TiO_2, MnO_2-CeO_2-TiO_2 and MnO_2-Fe_2O_3-CeO_2-TiO_2 which are denoted as MT, MCT and MFCT herein, respectively. Only a MnO_2-Fe_2O_3-CeO_2-TiO_2 catalyst was prepared with the impregnation method, which had the same composition of metal oxides as MFCT and was denoted as IMP-MFCT for differentiation with the MFCT. The mass ratios of metal oxides adopted for MnO_2-TiO_2, MnO_2-CeO_2-TiO_2 and MnO_2-Fe_2O_3-CeO_2-TiO_2 catalysts were 8.24/91.76, 8.24/16.29/75.37 and 8.24/10/16.29/65.37, respectively. The impregnation of $(NH_4)_2SO_4$ onto MFCT used an ammonium sulfate solution as the precursor, and the prepared sample was finally dried in air of 100 °C for 6 h.

The precursor reagents for the catalyst IMP-MFCT were industrial anatase nano-TiO_2, manganese acetate, ferric nitrate and cerium nitrate, and these chemicals provided the support and the metals Mn, Fe and Ce, respectively. For the catalysts made with the sol–gel approach the tetrabutyl titanate was employed as the Ti source, while the other precursors were the same as for the impregnation case. In the adopted sol–gel method, the sols were gelatinized at room temperature using surfactant-dissolved ethanol as the solvent. After stirring for 1 h, the required catalyst precursors were added into the sol, and this was succeeded with agitation for 48 h with dropwise addition of water–ethanol solvent. The resulting gel was finally dried at 80 °C and calcined at 400 °C for 3 h in air atmosphere to convert the gel into catalyst.

2.2. Catalyst characterization

Specific surface area, pore volume and pore size distribution of the catalysts were measured using nitrogen adsorption at 77 K and determined by the BJH method using an automated gas sorption system, Autosorb-1 (Quantachrome, NOVA1200). Prior to the measurement of the surface area and pore size distribution, the sample was degassed in vacuum at 623 K for 24 h. X-ray diffraction patterns were obtained in the 2θ angle range of 2–90° using nickel filtered Cu–K α radiation (λ = 0.15418 nm). XPS was used to analyze the atomic surface concentration on the tested catalyst. The spectra were recorded on a PerkinElmer Model 5300 X-ray photoelectron spectrometer using MgK_α (1253.6 eV) as a radiation source at 300 W and in the fixed analysis transmission mode with pass energies of 89.45 and 35.75 eV for the survey and high resolution spectra, respectively. Catalyst powder was put onto the sample holder and degassed overnight at room temperature at a pressure of 10^{-7} torr. Binding energies (BE) were measured for C 1s, O 1s Ti 2p, Mn 2p, Ce 3d, Fe 2p and S 1s. Sample charging effects were eliminated by correcting the observed spectra with the C 1s binding energy value of 284.6 eV. An estimated error of 0.1 eV can be considered for all the measurements. The spectra were smoothed through subtracting a nonlinear background. The microscopic features of a catalyst sample were observed also in the field-emission scanning electron microscope (FESEM, JSM-6700F of JEOL) running at 10 kV, the field-emission transmission electron microscope (FETEM, JEM-2010F of JEOL) running at 200 kV, and the scanning transmission electron microscope (STEM, JSM-6700F of JEOL) equipped with transmission electron detector and operated at 25 kV. The sulfate and ammonium group in a catalyst sample were detected with a Bruker Vector FTIR spectrometer that had a resolution of 2 cm^{-1} and used a DTGS (deuteriotriglycine sulfate) detector. For this measurement, the self-supporting wafer of 1.3 cm in diameter was prepared via pressing a mixture of the catalyst sample and a KBr salt at a specified mass ratio, and this wafer was in turn loaded into an IR cell equipped with a BaF2 window. The OPUS spectroscopic software was used in the FTIR analysis. The used TG analyzer was made by Seiko Co., and a AMTEK-made process mass spectroscopy (MS) was coupled to the TG analyzer to monitor the TG-effluent gas composition.

2.3. Catalyst evaluation

Evaluation of the activities of all the tested catalysts was performed in a fixed bed reactor by a programmed temperature rise at a heating rate of 5 °C/min. Mass flow meters controlled the flow rates of all employed reactant streams including NH_3-N_2, NO-N_2, SO_2-N_2 and O_2-N_2. In order to prevent formation of ammonium sulfite at the inlet of the reactor, the tubes connected to the reactor was all heated with tape heaters.

Simulated flue gas containing 600 ppm NO, 300 or 900 ppm SO_2 (when needed) and 2 vol.% O_2 was adopted. All tests were at a total flow rate of 400 mL min^{-1} and a NH_3-to-NO molar ratio of 0.8. The typical temperature used in assessing the low-temperature activity of the catalysts was 240 °C. At this temperature the residence time of gas in the reactor was about 0.15 s or the gas hourly space velocity (GHSV) was roughly 24,000 h^{-1} (room temperature). The concentrations of NO and N_2O in the inlet and outlet streams of the reactor were monitored using an on-line ABB flue gas analyzer. The conversion of NO was calculated by

$$NO_{Conversion} = \frac{C^i_{NO} - C_{NO}}{C^i_{NO}} \times 100\%,$$

where C^i_{NO} and C_{NO} refer to the NO concentration at the reactor inlet and outlet, respectively.

3. Result and discussion

3.1. Catalyst characterization

Table 1 shows that all the sol–gel catalysts have a surface area of about 200 $m^2\,g^{-1}$ and a pore volume of about 0.33 mL g^{-1}, which are obviously higher than the surface area of 79 $m^2\,g^{-1}$ and pore volume of 0.03 mL g^{-1} for the catalyst IMP-MFCT. This difference in the surface properties reflects rightly the different ways of pore formation for the sol–gel and impregnation catalysts. For IMP-MFCT, the pore resulted mainly from the inter-particle voids, whereas the removal of the structure directing agent (SDA) would cause the sol–gel catalysts to have meso pores and mesoporous structure. Fig. 1 compares the nitrogen adsorp-

Table 1
BET analysis results for fresh and spent catalysts referred to in this article.

Catalyst	BET surface area ($m^2 g^{-1}$)	Pore volume ($cm^3 g^{-1}$)	Average pore diameter (nm)
TiO_2	210.72	0.3572	7.2
MT	220.64	0.3433	7.5
MCT	200.69	0.3152	6.9
MFCT	197.87	0.3285	6.7
IMP-MFCT	79.25	0.03	<2
MFCT (16 h)	180.82	0.3065	7.0
MFCT (60 h)	180.65	0.3014	7.1

tion–desorption isotherms for the catalysts MFCT and IMP-MFCT, demonstrating an obvious hysteresis loop for MFCT when lowering the relative N_2 partial pressure from 0.8 to 0.45. For IMP-MFCT, however, there was almost no hysteresis detectable. The result just verified that the MFCT catalyst had a mesoporous structure, whereas the similar structure was not present in IMP-MFCT.

Fig. 2 shows that the XRD analysis produced obvious diffraction peaks only for the impregnation catalyst IMP-MFCT in 2θ angles varying from 5° to 90°. The weak X-ray diffraction characteristics of MCFT suggested that this catalyst would be inherently amorphous in structure, and all metal components (Mn, Ce, Fe) were highly dispersed. For IMP-MFCT, the distinctively obvious diffraction peaks appeared only for the anatase and oxides CeO_2 [7], MnO_2 [14] and Fe_2O_3 [8], revealing that all the metal components are presented as crystal grain on the anatase TiO_2 support. The inset figure of Fig. 2 mentions a diffraction peak for MFCT at $2\theta = 2°$. The shape of this peak indicated that a disordered mesoporous structure was formed in the sol–gel catalyst MFCT.

Fig. 3 shows the Ti 2p, O 1s, Mn 2p, Fe 2p, Ce 3d and S 2p photoelectron peaks of the MFCT and IMP-MFCT catalysts measured by XPS. The binding energies of Ce 3d and Ti 2p were similar for both the catalysts, but the energy of O 1s for IMP-MFCT exhibited two peaks at 529.7 and 531.5 eV for a main and a shoulder peak, respectively. Thus, there were at least two sorts of metal oxides on the surface of IMP-MFCT. For the MFCT catalyst, its binding energy of O 1s showed only one peak at 530.1 eV, implicating that the metal oxides were presented as a uniform compound like a solid solution. The binding energies of Mn 2p 3/2 and Mn 2p 1/2 were respectively 641.5 and 653.4 eV, which indicated probably the Mn^{4+} state [15]. In comparison with IMP-MFCT, there were obviously large intensity as well as sharpening in Mn 2p spectra for MFCT, suggesting that the dispersion or surface atomic concentration of Mn on the catalyst support surface (TiO_2) was higher for MFCT than for IMP-MFCT [14]. Conversely, as shown in Fig. 3, the intensity and sharpening of the binding energy for Fe 2p spectra were larger for IMP-MCFT, implying a lower surface atomic concentration of Fe for MFCT.

The atomic ratios of Mn 2p, Ce 3d and Fe 2p with respect to Ti 2p shown in Tab. 2 can be taken as a measure of the relative dispersion of the oxides of these metals on the TiO_2 support surface. The higher ratio implicates the better dispersion and higher surface concentration. Table 2 reveals that in comparison with IMP-MCFT the MFCT catalyst had higher surface atomic ratio for Mn, equivalent ratio for Ce and lower ratio for Fe, indicating that Mn was dispersed better on TiO_2 of MCFT to enable thus the higher Mn concentration on this catalyst surface. The differences in the mentioned surface atomic ratios between IMP-MFCT and MFCT might be attributed to the different interactions of metal oxides with TiO_2 support in their associated catalyst preparation processes. For example, the higher atomic ratio or concentration of Fe on the surface of IMP-MFCT might be a result from the non-uniform catalyst structure and the decomposition of ferric nitrate at low temperatures, while the high atom ratio of Mn for MCFT was possibly related to the strong oxidation ability of Mn, which facilitated the depletion of the employed organic SDA to expose the metal element itself in calcining the catalyst.

Figs. 4 and 5 present the electron microscopic images at different magnifications for MFCT and IMP-MFCT. The SEM images in Fig. 4 demonstrate that the surface of the MFCT catalyst was smoother and more compact than that of IMP-MFCT. As shown in Fig. 4(b3), the IMP-MFCT catalyst was in fact a kind of agglomeration of nano- to micro-size particles. These surface features comply with the demonstration in Fig. 5 through TEM images that identified an amorphous structure for MFCT and a crystal structure for IMP-MFCT. The average space between the aligned crystal lattices of IMP-MFCT was found to be about 0.21 nm in Fig. 5(b1), while the active components were observed to interlace obviously on the MFCT catalyst surface in Fig. 5(a2). The latter indicated in fact that the active components in MFCT were highly uniformly dispersed and closely interacted.

3.2. Performance in low-temperature SCR

Fig. 6 shows the NO conversion over all the tested catalysts realized in varying the reaction temperature from 100 to 400 °C. With raising temperature the realized NO conversion first increased and then decreased, making all the catalysts have a relatively stable NO conversion in between. The temperature range for such a steady NO conversion refers to the activity temperature window of the catalyst. Fig. 6 demonstrates that the catalyst MFCT had the widest temperature window of about 200–400 °C, while

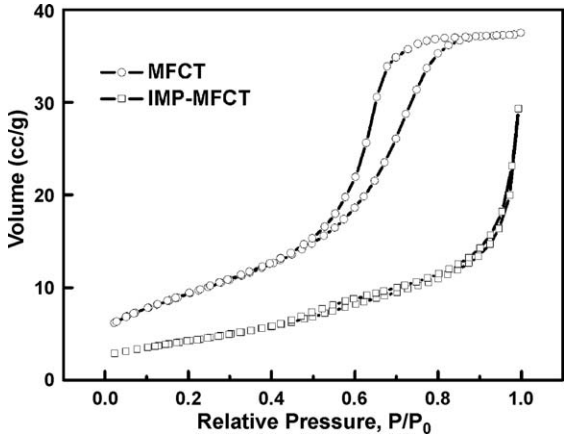

Fig. 1. N_2 adsorption–desorption isotherms for MFCT and IMP-MFCT catalysts.

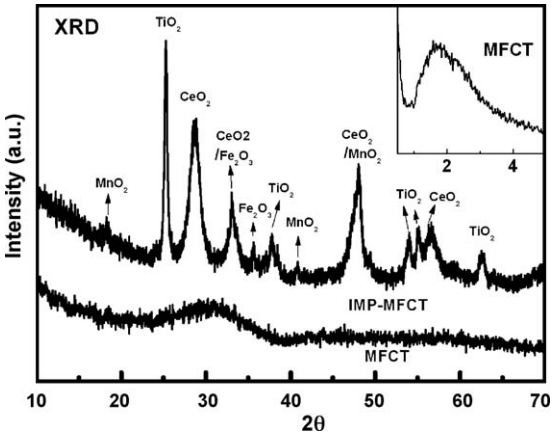

Fig. 2. XRD patterns of fresh MFCT and IMP-MFCT catalysts.

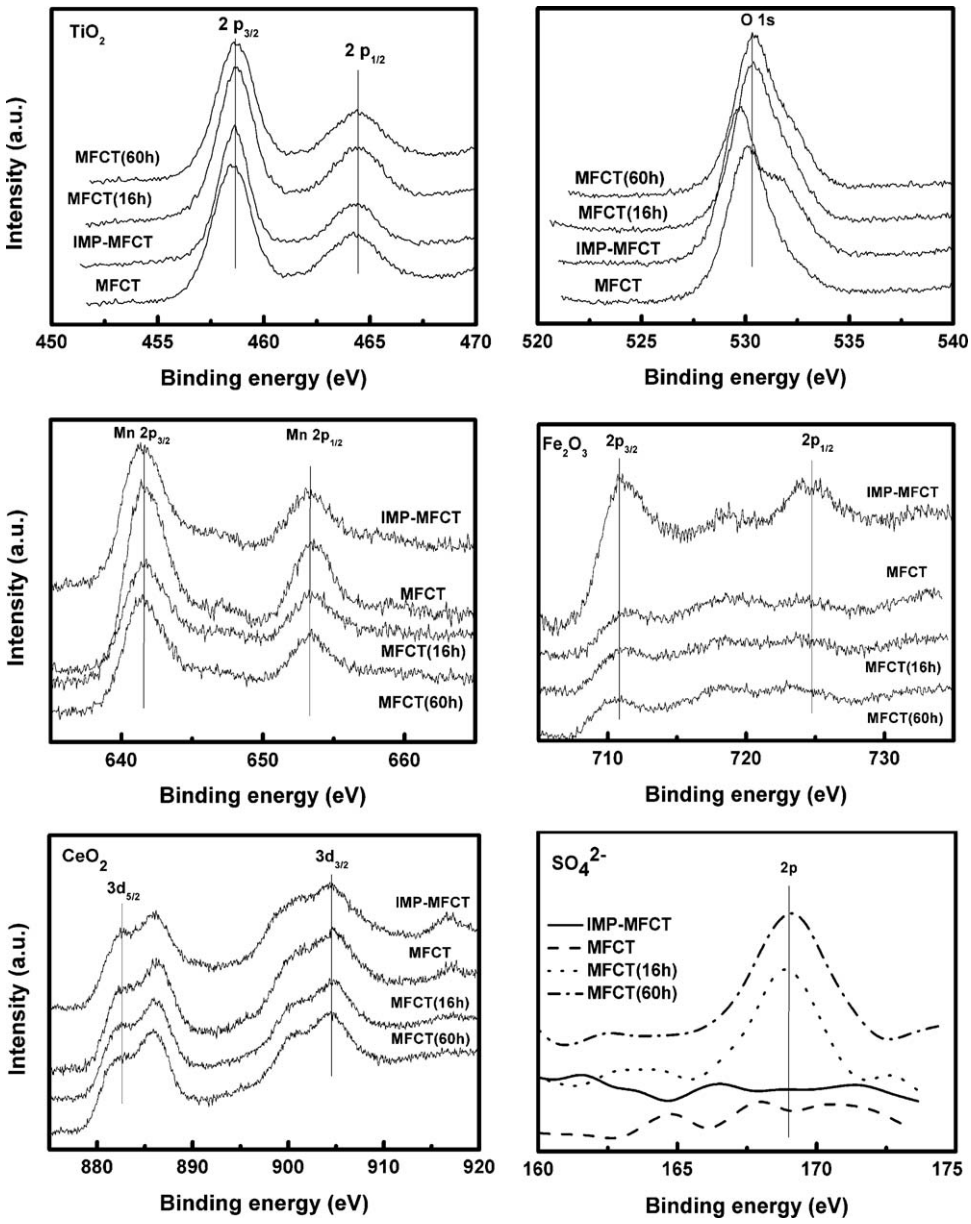

Fig. 3. XPS of Mn 2p, Fe 2p, Ce 3d and S 2p core level peak for the catalysts IMP-MFCT, MFCT, MFCT (16 h) and MFCT (60 h), here MFCT (*x* h) represents spent MFCT catalyst on stream for *x* hours in the gas containing SO_2 of 300 or 900 ppm tested later in Figs. 10 and 11.

the IMP-MFCT catalyst enabled acceptable NO conversions of over 80% only in 200–300 °C at an NH_3/NO ratio of 0.8. Pure TiO_2 had very low activity, whereas dispersing Mn onto TiO_2 (i.e. MT) resulted in distinctively improved activity for SCR of NO (top conversion being over 80%). The result clarifies that Mn was the activity metal for all the tested catalysts. Of the Mn-containing catalysts, MT exhibited the lowest activity and reached its peak activity at about 270 °C. This temperature for realizing the peak activity was much higher than that for the other catalysts, which was about 210 °C. The results demonstrate that the addition of Ce greatly improved the low-temperature activity of the catalysts. Overall, Fig. 6 clarifies that the catalyst MFCT provided the best performance for SCR of NO with NH_3. Although IMP-MCFT had higher activity at temperatures until 200 °C, but it was easiest to deactivate at rather high temperatures. Combining these with the XRD and XPS analysis results presented above, one can derive that the inferior dispersion of active component and the formation of crystal grains on the catalyst surface would make the catalyst's oxidative ability too strong to maintain the desired high catalytic activity at low temperatures and fast activity deactivation at high temperatures. This is why the activity temperature window of IMP-MCFT was much narrower than that of MFCT. Fig. 6 reveals that the realized peak NO conversions were above 0.8, the adopted NH_3-to-NO ratio, suggesting that non-stoichiometry reaction between NO and NH_3 into N_2 likely occurred [16], or the adsorbed NH_3 which was released at

Table 2
Surface atomic ratios of Mn 2p, Ce 3d and Fe 2p with respect to Ti 2p for the catalysts IMP-MFCT, MFCT, MFCT (16 h) and MFCT (60 h).

Catalyst	Mn/Ti	Ce/Ti	Fe/Ti
MFCT	0.26	0.17	0.01
IMP-MFCT	0.20	0.18	0.12
MFCT (16 h)	0.18	0.16	0.03
MFCT (60 h)	0.17	0.17	0.03

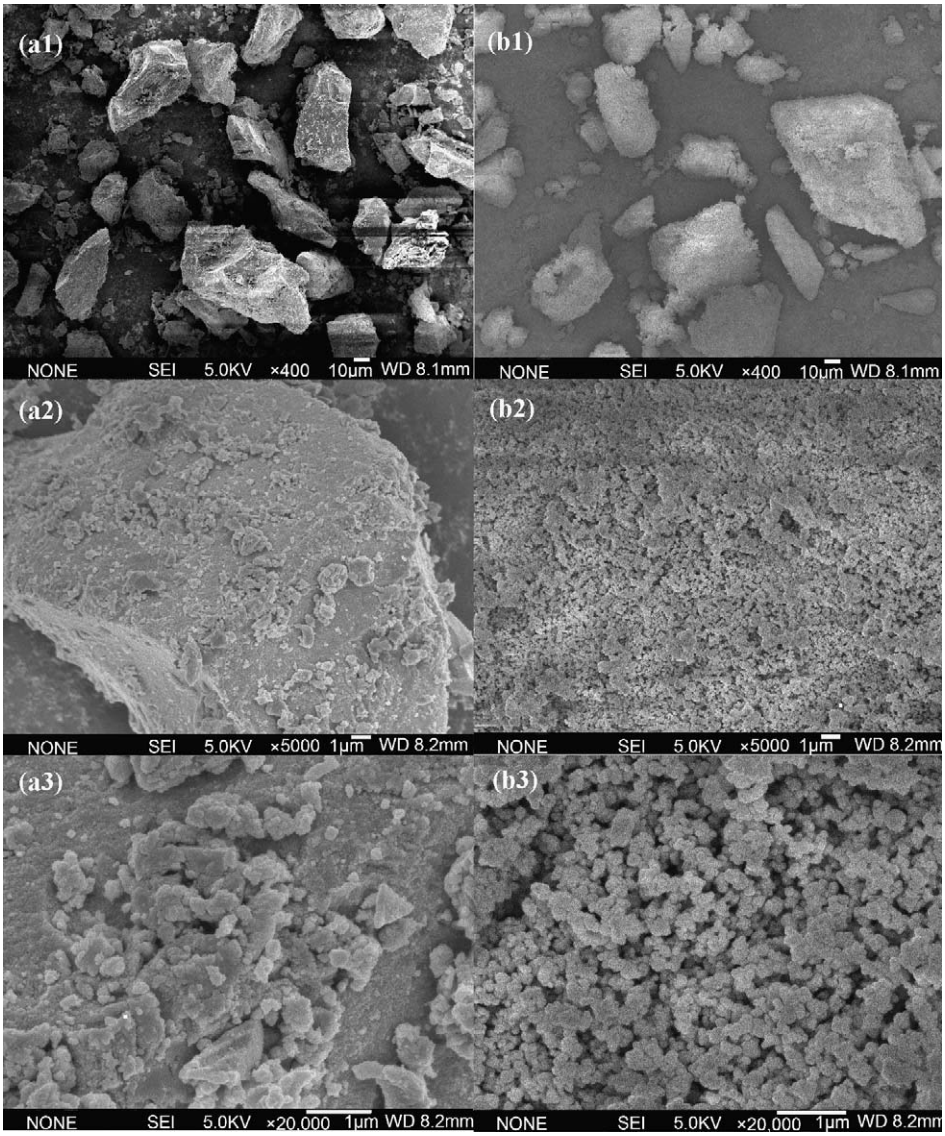

Fig. 4. SEM images at different magnifications for catalysts (a) MFCT and (b) IMP-MFCT.

relatively high temperatures led the actual NH_3/NO ratios to be over 0.8.

Fig. 7 compares the N_2O concentrations in the effluent gases of the tests mentioned in Fig. 6 over all the TiO_2-supported Mn catalysts. There was an obvious formation of N_2O over IMP-MFCT, whereas no N_2O formation was detected until 300 °C for all the sol–gel catalysts. The effluent N_2O concentration over IMP-MFCT first increased with increasing temperature and in turn remained in a constant of about 100 ppm when the temperature was higher than 250 °C. The highest effluent N_2O concentration over the sol–gel catalysts appeared in 300–400 °C but was lower than 20 ppm. Particularly, over the MCFT catalyst there was almost no N_2O formation until 400 °C. These clarify in fact that the sol–gel approach, in comparison with the impregnation method, greatly increased the selectivity of the resulting catalyst for SCR of NO into N_2. The different N_2O concentrations for MT, MCT and MFCT in Fig. 7 demonstrated further that the inclusion of Ce into the catalyst increased slightly the N_2O formation, while the addition of Fe allowed conversely a great suppression of the N_2O formation.

During SCR of NO via NH_3 the formation of N_2O should be attributed to the oxidation of NH_3. Thus, Fig. 8 tested further the oxidation of a gas containing 480 ppm NH_3 via 2% O_2 over the catalysts MFCT and IMP-MFCT. The overall tendency is that the oxidation of NH_3 was likely into N_2O at low temperatures and into NO at high temperatures. On IMP-MFCT, as shown in Fig. 8(b), obvious formation of N_2O was identified until 400 °C but it was peaked at about 230 °C. The formation of NO over this catalyst started at about 340 °C and in turn rapidly increased with raising the reaction temperature. Comparing to this, over MFCT there was much weak oxidation of NH_3 into N_2O and NO. The formation of N_2O became detectable only at temperatures over 340 °C, while the formed NO was very limited until 400 °C.

Because the catalysts MFCT and IMP-MFCT had the same composition, the preceding results clarified by Fig. 8 reveal in fact that the catalyst structure is determinative of the oxidation activity to NH_3. Concretely, the highly dispersed MnO_2 and large surface area of MFCT greatly suppressed the oxidation activity for NH_3. This is why the NO conversion in Fig. 6 rapidly decreased with raising temperature for IMP-MCFT when the temperature became certainly high, whereas the MFCT allowed a much wide activity temperature window (Fig. 6) and a good selectivity of SCR of NO into N_2 (Fig. 7). Also because of its strong oxidation activity for NH_3, the IMP-MFCT catalyst enabled higher NO conversion at temperatures below 200 °C in Fig. 6. The differences between the

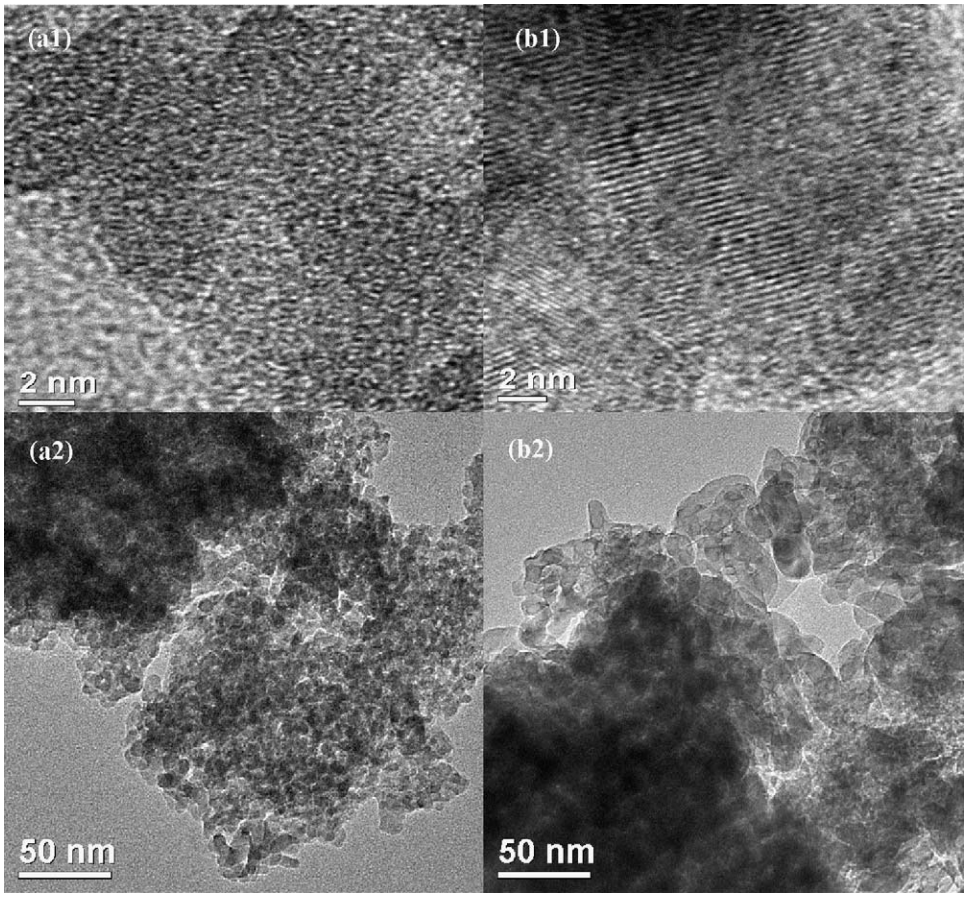

Fig. 5. TEM images at different magnifications for catalysts (a) MFCT and (b) IMP-MFCT.

IMP-MFCT and MFCT catalysts in the dispersion of active components and the interaction of metal oxides on the catalyst surface might be responsible for their different activities demonstrated above.

3.3. Resistance to steam or SO_2 poisoning

Fig. 9 shows the resistance of all the tested TiO_2-supported Mn catalysts to steam poisoning in 2 h and then to SO_2 poisoning during SCR of NO with NH_3. All the catalysts manifested high catalytic activity to lead to NO conversions higher than 85% in the absence of SO_2. Once steam was introduced into the flue gas, the NO conversions over all the catalysts exhibited first a peak value and then decreased to a steady value. The possible reason for the NO conversion increase at the first stage might be the dilution effect of steam. Comparatively, the introduction of steam only slightly reduced the NO conversions over the sol–gel catalysts, implicating that the MCFT catalyst had much higher resistance to the poisoning or activity reduction of steam than the IMP-MFCT catalyst did. Many researchers have revealed that the competition adsorption of steam on catalyst's active sites decreased the NH_3 adsorption, which caused in turn the decrease in the realized NO

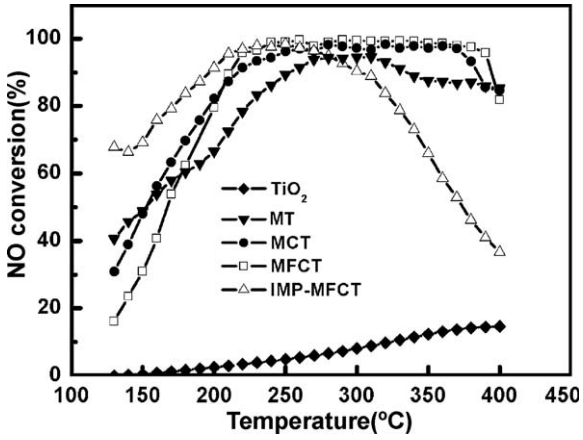

Fig. 6. NO conversion versus reaction temperature over different catalysts (NO = 600 ppm; NH_3/NO = 0.8; O_2 = 2%; N_2 as balance gas, GHSV: 24,000 h^{-1})

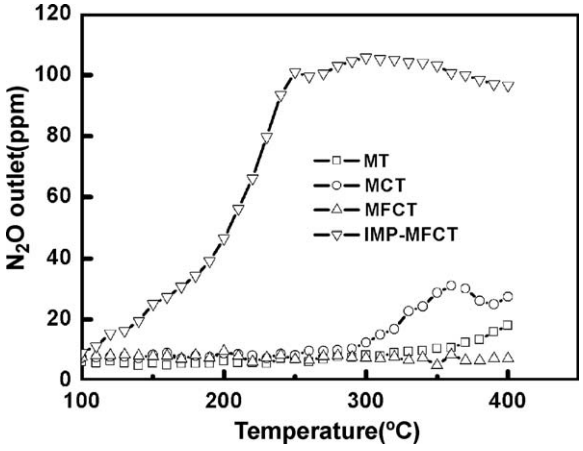

Fig. 7. Concentration of N_2O in the effluent gases corresponding to the tests. Shown in Fig. 6 (test conditions are in Fig. 6)

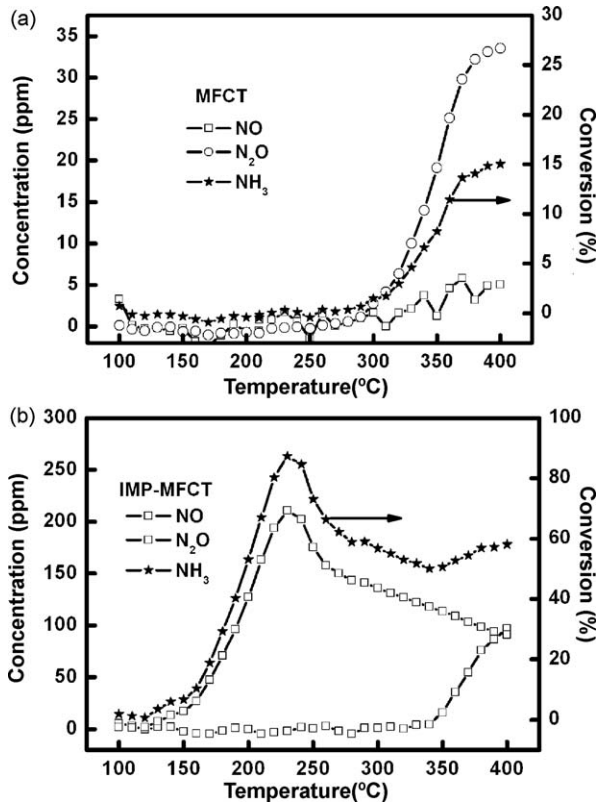

Fig. 8. The trends of forming NO and N_2O in oxidizing NH_3 on MFCT and IMP-MFCT catalysts (NH_3: 480 ppm; O_2: 2%; N_2 as balance gas; GHSV: 24,000 h^{-1}).

conversion [17,18]. As a consequence, the good resistance of all the sol–gel catalysts to the steam poisoning would justify that these catalysts possessed better hydrophobicity or had more active sites than the IMP-MFCT catalyst.

Once SO_2 was further introduced into the treated flue gas, the NO conversion over all the catalysts exhibited first a rapid decrease, demonstrating that the presence of SO_2 in the gas certainly reduced the catalyst activity. Nonetheless, for the catalysts MT, MCT and MFCT made with the sol–gel method their realized NO conversions finally stabilized themselves at 70%, 72% and 80%, respectively. Different from this, the NO conversion enabled by IMP-MFCT showed quick decreasing after SO_2 was introduced and in the tested 2.5 h the conversion dramatically

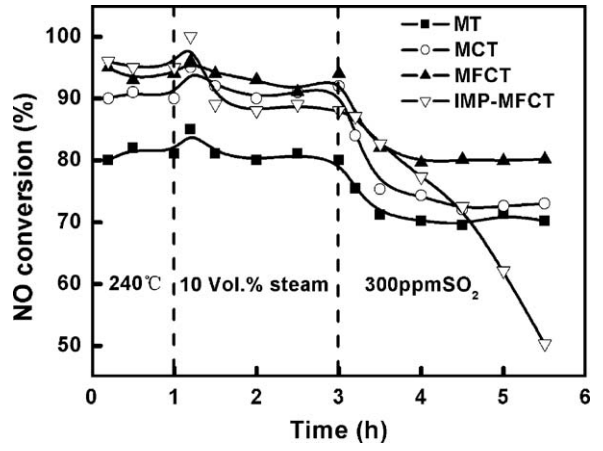

Fig. 9. Effect of steam or SO_2 on the activity of different Mn-base catalysts (H_2O: 10 vol.%, SO_2: 300 ppm, NO: 600 ppm, NH_3/NO: 0.8, O_2: 2%, N_2: balance gas, temperature: 240 °C, GHSV: 24,000 h^{-1})

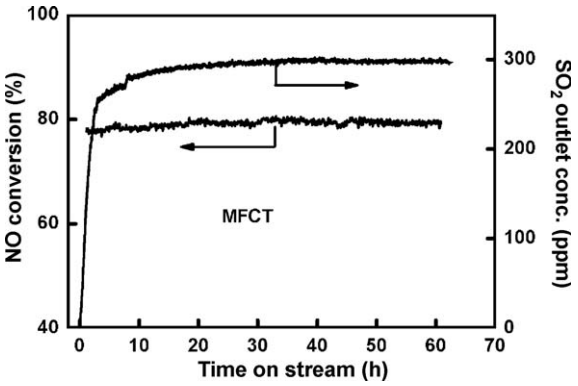

Fig. 10. Stability of 60-h test for SO_2-poisoning resistance of MFCT (SO_2: 300 ppm, NO: 600 ppm, NH_3/NO: 0.8, O_2: 2%, N_2: balance gas, temperature: 240 °C, GHSV: 24,000 h^{-1}).

decreased to 50% from about 90%. Therefore, the sol–gel approach granted the Mn-base catalyst not only good activity and selectivity (Figs. 6–8) but also greatly improved resistance to the poisoning of SO_2 containing in the treated flue gas.

The improved resistance to SO_2 poisoning of MFCT was demonstrated further in Fig. 10 through a long-time continuous test. In the tested 60 h in a flue gas containing 300 ppm SO_2 and 600 ppm NO, the realized NO conversion was constantly maintained at about 78% under the conditions of 240 °C, 24,000 h^{-1} GHSV and 0.8 NH_3-to-NO ratio. Fig. 9 shows also that the SO_2 concentration at the reactor exit finally reached its inlet level, demonstrating that little SO_2 was retained in the reactor.

Fig. 11 demonstrates further how a rather high SO_2 concentration of 900 ppm in flue gas inhibited the catalyst activity of MFCT and how the SO_2 concentration at the reactor exit changed during the test. It is obvious that increasing the SO_2 concentration to 900 ppm from 300 ppm did not obviously vary the realized NO conversion over the MFCT catalyst, demonstrating further its pretty good resistance to the SO_2 poisoning. Fig. 11 mentions also that the SO_2 concentration measured at the reactor exit exhibited a slow increase (in 4 h) before it approached a stable value equal to that measured at the reactor inlet. This should indicate the formation of ammonium sulfate in the reactor, as will be shown further through characterizing the spent catalyst, but the final approach of the inlet SO_2 concentration suggested that there was possibly a dynamic balance between the formation and decomposition of ammonium sulfate on the catalyst surface. The adsorbed SO_2 on the catalyst surface was proved to be easily oxidized over MnO_x, while the coexisting with NO_x would further facilitate this

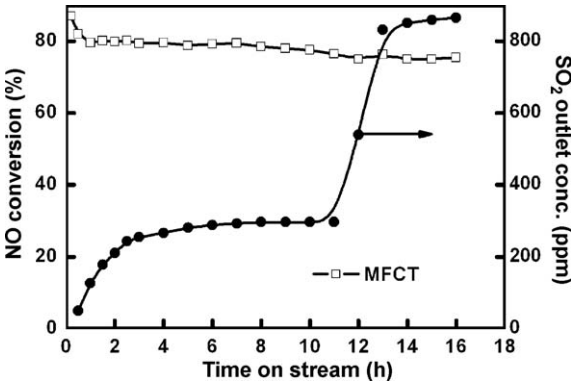

Fig. 11. Effect of SO_2 concentration over Mn-Fe-Ce-TiO_2 catalyst (SO_2: 300 or 900 ppm, NO: 600 ppm, NH_3/NO: 0.8, O_2: 2%, N_2: balance gas, temperature: 240 °C, GHSV: 24,000 h^{-1}).

oxidation (such as $NO_2 + SO_2 \rightarrow NO + SO_3$). These lead to the formation of ammonium sulfate via the reaction between SO_3 and NH_3 and in turn to the inhibition effect of SO_2 on the denitration activity of the Mn-base catalyst. For MCFT, a dynamically balanced ammonium sulfate formation and decomposition is realized, enabling consequently its good resistance to SO_2 poisoning as shown in Figs. 9–11.

3.4. Result justification

Fig. 12 shows the weight loss and effluent gas composition of a few typical catalysts tested in a TG coupled to a online mass spectrometer. The catalysts included the fresh MFCT, spent MFCT (16 h) and MFCT (60 h) and $(NH_4)_2SO_4$ impregnated on the fresh MCFT according to a ratio of 10 wt.%, here the MCFT (*x* h) refers to a spent catalyst tested in a SO_2-contaning flue gas for *x* hours (see Figs. 10 and 11). The heating rate for TG was 10 °C/min.

As shown in Fig. 12(a), the TG curves revealed two weight-loss stages for all the catalysts. While the first indicated a small weight loss at 250–350 °C, the latter revealed a large weight loss at 700–850 °C. Matching to the off-gas composition for MFCT (60 h) in Fig. 12(b) measured by MS, one can believe that the first and second weight losses corresponded to the decompositions of ammonia sulfate and $MnSO_4$, respectively. These features of TG and off-gas composition variations for the spent catalysts consisted well with the findings of Kijlstra et al. [19] obtained in investigating the deactivation of MnO_x/Al_2O_3 catalyst in SO_2-containing flue gas. They concluded that the formation of metal sulfate, such as $MnSO_4$ and $Al_2(SO_4)_3$, was the critical cause for their identified catalyst deactivation (or poisoning).

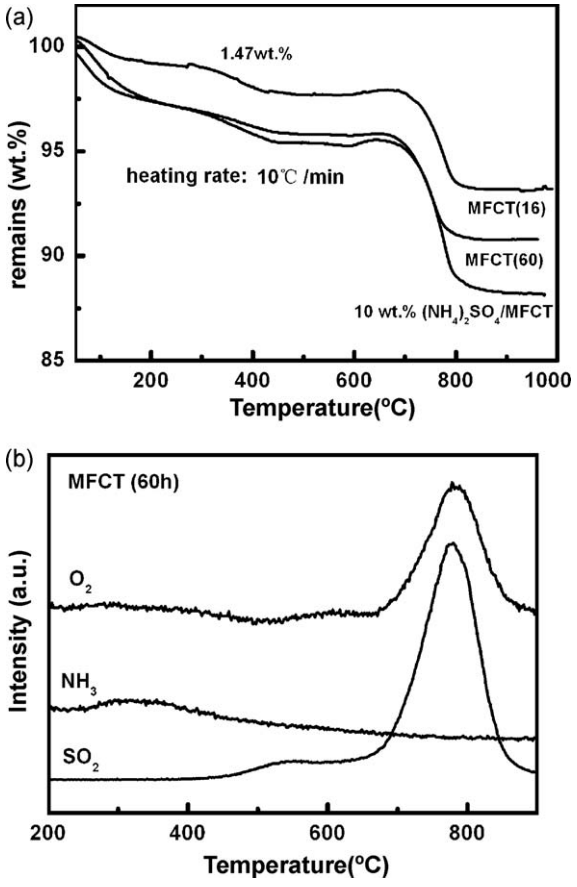

Fig. 12. TG analyses at 10 °C/min for spent catalysts MFCT (16 h) and MFCT (60 h) and for 10 wt.% $(NH4)_2SO_4$ impregnated on MFCT with the off-gas measured by MS [but shown only for MFCT (60 h) in (b)].

In Fig. 12, the total weight losses between 250 and 850 °C for the catalysts MFCT (16 h) and MFCT (60 h) were 6.04 and 6.50 wt.%, respectively. This little difference in the weight loss verifies further that the MCFT catalyst has stable resistance to SO_2 poisoning. Otherwise, the weight loss of MCFT (60 h) would be obviously higher than that of MCFT (16 h).

In order to identify how the metal sulfates (here $MnSO_4$) are formed on the catalyst surface, the impregnated $(NH_4)_2SO_4$ (10 wt.%) on fresh MCFT catalyst was tested using TG under the same temperature program as applied to the spent catalyst TG tests. The resulting TG curve in Fig. 12 exhibited the similar two types of weight losses, an experimental result similar to the observation of Tong et al. [13] and suggesting that the released SO_3 from $(NH_4)_2SO_4$ decomposition at lower temperatures combined with the catalyst Mn species to form $MnSO_4$ during the heating process. This implies that the identified $MnSO_4$ decomposition in Fig. 12 via TG for the spent catalyst at 700–850 °C should also come from the decomposition of deposited $(NH_4)_2SO_4$ at lower temperatures, and it does not indicate that $MnSO_4$ was definitely formed by the reaction between the oxidized SO_2 and catalyst Mn species during SCR.

The XPS spectra of MFCT (16 h) and MFCT (60 h) shown in Fig. 3 can be analyzed to identify further the species causing SO_2 poisoning. Comparing to the spectra of fresh MCFT catalyst, the spectrum intensity of Mn 2p became smaller after reactions in SO_2-containing gas to indicate a decrease of the Mn surface atomic concentration. Nonetheless, the binding energy of Mn 2p remained constantly at 641.5 eV, indicating that MnO_2 rather than $MnSO_4$ stably existed on the surface. Therefore, slight deactivation of MFCT after introducing SO_2 into the flue gas should be mainly due to the deposition of ammonium sulfate on the active site (MnO_2) rather than the formation of $MnSO_4$ (otherwise, Mn^{2+} should be obviously detected in the XPS analysis) Fig. 3 shows also that the intensity of S 2p at a bending energy of 169.1 eV had little difference for MFCT (60 h) and MFCT (16 h), revealing that the relative amount of sulfate did not obviously increase in increasing the reaction time from 16 to 60 h. This further verifies the stability of the catalyst and its activity in SO_2-contaning gas.

Nonetheless, the surface atomic ratio between Mn 2p and Ti 2p in Table 2 decreased to 0.19 from 0.26 after reacting for 16 h in a SO_2-contaning gas, and further declined to 0.18 in the extended reaction period from 16 to 60 h. Comparing to this, the ratios for Fe 2p and Ce 3d against Ti 2p changed little in the tested 60 h. Consequently, the presence of SO_2 in the reactant gas decreased really the surface concentration of Mn atom through the deposition of ammonium sulfate (rather than the formation of $MnSO_4$ because Mn^{2+} did not obviously identified in XPS spectra), but the speed of decreasing the Mn surface concentration and in turn the catalyst activity tended to become stable with increasing the SCR reaction time.

In summary of the above analyses, one can believe that the decomposed metal sulfates for MCFT (16 h) and MCFT (60 h) shown in Fig. 12 might be mainly related to the decomposition of $(NH_4)_2SO_4$ at lower temperatures, and for the MCFT prepared in this article very little metal sulfate was in fact formed during SCR (for 60 h) over the catalyst in SO_2-contaning gases.

Fig. 13 shows the FT-IR spectra of several fresh and spent catalysts. The spent catalysts were from tests in flue gas containing SO_2. All catalysts exhibited vibration absorptions centering at wave numbers of 1625, 626 and 770 cm^{-1}. These absorptions featured different metal oxides. In comparison with the fresh MFCT, the spent catalyst had a new absorption at 1414 cm^{-1} to indicate the presence of NH_4^+ species, such as $(NH_4)_2SO_4$, that were chemisorbed on the Brønsted acid sites [20,21]. Meanwhile, there was also an absorption at 1140 cm^{-1} for all the spent catalysts, showing the existence of SO_4^{2-}. Free SO_4^{2-} ion has usually two infrared absorptions at 1140 and 626 cm^{-1} [22], but the absorption at 626 cm^{-1} was overlapped by the absorptions of TiO_2, which was

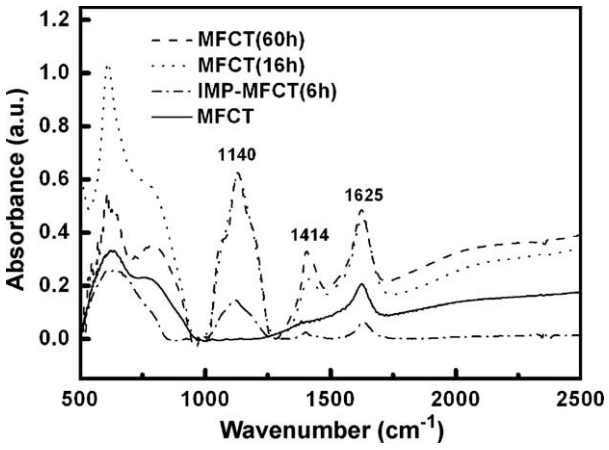

Fig. 13. FT-IR spectrum of a few typical fresh and spent catalysts.

easily influenced by the preparation method and impurities [23]. These results of FTIR analysis were consistent with Zhu et al. [24] and demonstrated that the inhibitory effect of SO_2 was surely due to the formation of ammonium sulfate which deposited on the active sites and blocked the active channels of catalyst.

The IR absorption intensity at 1140 cm^{-1} showed little difference between MFCT (16 h) and MFCT (60 h) but this absorption was evidently larger than that for IMP-MFCT (6 h). Against these, the fresh MFCT had almost no IR absorption at 1140 cm^{-1}. At 1414 cm^{-1}, the identified IR absorption intensities were subject to an order of MFCT (60 h)≥MFCT (16 h) ≫ IMP-MFCT (6 h) > MFCT. These results demonstrate that within the tested 60 h the amount of deposited ammonium sulfate slightly increased with lengthening the reaction time. Although having slightly more ammonium sulfate deposited, the catalyst MFCT was not much deactivated in Fig. 8, whereas the IMP-MFCT was quickly deactivated at rather low ammonium sulfate deposition. Hence, the MFCT catalyst, comparing to IMP-MFCT, had obviously large capacity to resist the poisoning resulting from ammonium sulfate. This enabled consequently the good low-temperature activity of MFCT shown in Fig. 8 for SO_2-cotaining flue gas.

Table 1 shows further that both MFCT (16 h) and MFCT (60 h) had similar surface area and pore volume that were lower than that for fresh MFCT. This complies with the preceding demonstration that ammonium sulfate was formed and deposited on the catalyst in SCR reactions. Nonetheless, the little difference in ammonium sulfate deposition between MFCT (16 h) and MFCT (60 h) shows that after certain time of reactions the deposition approached a stable state. This is also why in Fig. 11 the catalyst MFCT allowed steady NO conversion in SO_2-containing gas. The meso-pore structure of MFCT should be responsible for this property of the catalyst. The pores allowed quick diffusion of NO_x in catalyst to accelerate the decomposition of ammonium sulfate during SCR reactions, leading thus to a dynamic equilibrium between the deposition and decomposition of ammonium sulfate on the catalyst. For IMP-MFCT, however, the slow diffusion of NO in the catalyst makes the ammonium sulfate hardly decompose so that the deposition is always quicker than the decomposition to cause consequently the catalyst to continuously deactivate.

4. Conclusions

One-pot prepared mesoporous MnO_2-Fe_2O_3-CeO_2-TiO_2 catalyst according to the sol–gel approach exhibited high dispersion of active components in the catalyst and high surface area. Comparing with the same-composition catalyst made with the impregnation method, the mesoporous catalyst exhibited good low-temperature activity in SCR of NO with NH_3, low N_2O escape, low oxidation to NH_3, good resistance to SO_2 poisoning and good activity stability. In a simulated flue gas containing 300 ppm SO_2 and 600 ppm NO, stable NO removals close to 80% were realized at 240 °C and an NH_3-to-NO ratio of 0.8 in a continuous SCR test for 60 h, whereas the activity of the impregnation catalyst decreased rapidly and continuously when SO_2 was included into the treated gas. XPS and FT-IR analyses of fresh and spent catalysts demonstrated that over the sol–gel catalyst prepared in this article there were very limited formation of metal sulfate during SCR of NO with NH_3 at about 240 °C, and the deposition of ammonium sulfate on the catalyst appeared to be the dominant cause for the deactivation or activity reduction in SO_2-contaning gases. The mesopores structure and metal oxides existing state present in the sol–gel catalyst were suggested to facilitate greatly the decomposition of ammonium sulfate deposited on the catalyst during SCR reactions. This made the decomposition of ammonium sulfate quick enough to reach possibly a dynamic balance with the deposition of the sulfate to allow consequently the sol–gel catalyst a stable SCR activity in SO_2-containing flue gases. The article investigated also how the Fe and Ce elements affected the catalyst activity and its resistance to the poisoning of SO_2, clarifying further that the catalyst structure rather than the catalyst composition dominates the catalyst's resistance to the poisoning of SO_2 during SCR of NO with NH_3.

References

[1] B. Stefan, H. Thomas, Appl. Catal. B 28 (2000) 101.
[2] S. Djerad, L. Tifouti, M. Crocoll, W. Weisweiler, J. Mol. Catal. A: Chem. 208 (2004) 257.
[3] S.T. Choo, S.D. Yim, I.S. Nam, S.W. Ham, J.B. Lee, Appl. Catal. B 44 (2003) 237.
[4] V.I. Pârvulescu, S. Boghosian, V. Pârvulescu, S.M. Jung, P. Grange, J. Catal. 217 (2003) 172.
[5] N. Macleod, R.M. Lambert, Catal. Lett. 90 (2003) 111.
[6] P.G. Smirniotis, D.A. Peña, B.S. Uphade, Angew. Chem., Int. Ed. 40 (2001) 2479.
[7] G.S. Qi, R.T. Yang, R. Chang, Appl. Catal. B 51 (2004) 93.
[8] G.S. Qi, R.T. Yang, Appl. Catal. B 44 (2003) 217.
[9] D.A. Pena, B.S. Uphade, P.G. Smirniotis, J. Catal. 221 (2004) 421.
[10] E. Garcia-Bordeje, A. Monzon, M.J. Lazaro, R. Moliner, Catal. Today 102–103 (2005) 177.
[11] Z.P. Zhu, Z.Y. Liu, S.J. Liu, H.X. Niu, Appl. Catal. B 23 (1999) L229.
[12] W. Sjoerd Kijlstra, Monty Biervliet, Eduardo K. Poels, Appl. Catal. B 16 (1998) 327.
[13] J.H. Huang, Z.Q. Tong, Y. Huang, J.F. Zhang, Appl. Catal. B 78 (2008) 309.
[14] P.R. Ettireddy, N. Ettireddy, S. Mamedov, et al. Appl. Catal. B 76 (2007) 123.
[15] F. Kapteijn, J. Dick van Langeveld, J.A. Mouljin, et al. J. Catal. 150 (1994) 94.
[16] IN-SIK NAM, J. Catal., 119 (1989) 269.
[17] M. Crocoll, S. Kureti, W. Weisweiler, J. Catal. 229 (2005) 480.
[18] G. Ramis, L. Yi, G. Busca, M. Turco, E. Kotur, R.J. Willey, J. Catal. 157 (1995) 523.
[19] W.S. Kijlstra, M. Biervliet, E.K. Poels, A. Bliek, Appl. Catal. B 16 (1998) 327.
[20] N.Y. Topsøe, Science 265 (1994) 1217.
[21] M. Takagi, T. Kawai, M. Soma, T. Onishi, K. Tamaru, J. Phys. Chem. 80 (1976) 430.
[22] K. Nakamoto, Infrared and Raman Spectra of Inorganic and Coordination Compounds, 4th ed., Wiley, New York, 1986.
[23] G. Ertl, H. Knozinger, J. Weitkamp, Handbook of Heterogeneous Catalysis, WILEY-VCH Company, Weinheim, 1997, p. 539.
[24] Z.P. Zhu, Z.Y. Liu, S.J. Liu, H.X. Niu, Appl. Catal. B 30 (2001) 267.